Journal of Zhejiang University-SCIENCE A (Applied Physics & Engineering)
ISSN 1673-565X (Print); ISSN 1862-1775 (Online)
www.zju.edu.cn/jzus; www.springerlink.com
E-mail: jzus@zju.edu.cn

Modeling droplet vaporization and combustion with the volume of fluid method at a small Reynolds number*

Xiao-bin ZHANG, Wei ZHANG, Xue-jun ZHANG†‡

(*Institute of Refrigeration and Cryogenics*, *Zhejiang University*, *Hangzhou 310027*, *China*)

†E-mail: xuejzhang@zju.edu.cn

Received Dec. 13, 2011; Revision accepted Feb. 6, 2012; Crosschecked Apr. 5, 2012

Abstract: The volume of fluid (VOF) formulation is applied to model the combustion process of a single droplet in a high-temperature convective air free stream environment. The calculations solve the flow field for both phases, and consider the droplet deformation based on an axisymmetrical model. The chemical reaction is modeled with one-step finite-rate mechanism and the thermo-physical properties for the gas mixture are species and temperature dependence. A mass transfer model applicable to the VOF calculations due to vaporization of the liquid phases is developed in consideration with the fluctuation of the liquid surface. The model is validated by examining the burning rate constants at different convective air temperatures, which accord well with experimental data of previous studies. Other phenomena from the simulations, such as the transient history of droplet deformation and flame structure, are also qualitatively accordant with the descriptions of other numerical results. However, a different droplet deformation mechanism for the low Reynolds number is explained compared with that for the high Reynolds number. The calculations verified the feasibility of the VOF computational fluid dynamics (CFD) formulation as well as the mass transfer model due to vaporization.

Key words: Droplet, Vaporization, Combustion process, Volume of fluid (VOF), Numerical simulation
doi:10.1631/jzus.A1100338 **Document code:** A **CLC number:** TQ038.3

1 Introduction

Fuel is usually sprayed into a cylinder of an internal combustion engine or into a gas turbine or jet engine combustion chamber where it burns. The combustion-generated heat is converted to mechanical work, and thus the exergy efficiency of the combustion process is a very important parameter. To conduct an exergy analysis, and to understand the combustion process in general, fundamental information on the temperature, the reaction speed and completeness, and factors affecting the rate of heat and mass transfer for a spray droplet are necessary (Lior *et al*., 2006). A number of numerical analyses of the unsteady combustion process of a spray droplet were indeed conducted (Renksizbulut and Haywood, 1988; Abramzon and Sirignano, 1989; Dash and Som, 1991; Haywood *et al*., 1994a; Shaygan and Prakash, 1995). The thermophysical properties of the gas mixture were calculated by methods ranging from the "1/3 rule" (Abramzon and Sirignano, 1989; Jog *et al*., 1996; Dgheim *et al*., 2002) to those considering temperature and concentration dependence (Haywood *et al.*, 1994a; 1994b). Various assumptions must typically be made to simplify the numerical solutions of the models that characterize the multi-physical transient behavior of the droplet vaporization and combustion process (Jog *et al*., 1996; Dgheim *et al*., 2002; Cuoci *et al*., 2005). A good example was the assumption of no liquid phase motion and chemical reaction in the gas mixture (Renksizbulut and Yuen, 1983). Madooglu and Karagozian (1993) developed a boundary-layer approximation, where all effects associated with viscosity and chemical reaction were assumed to be confined to a viscous layer adjacent to the droplet surface.

‡ Corresponding author

* Project supported by the National Basic Research Program (973) of China (No. 2011CB706501), and the Fundamental Research Funds for the Central Universities (No. 1A4000*172210101[67]), China

One of the main difficulties for modeling droplet combustion is the presence of internal 2D circulation inside a fuel droplet, which has a strong influence on the vaporization process and greatly increases the computational complexity. A frequently used approach is to assume that the circulation can be represented as a Hill's spherical vortex (Abramzon and Sazhin, 2005) with a uniform droplet surface temperature, thus the heat transferred into the interior of the droplet can be modeled by an effective heat conductivity, which is either a constant (Talley and Yao, 1988) or depends on the liquid Peclet number (Abramzon and Sirignano, 1989). To accurately model the circulation, more complicated models considering the flow and heat transfer for both liquid and gas phases, combined with variable physical properties as well as chemical reaction, have also been developed (Dash and Som, 1991; Chiang *et al*., 1992; Dgheim *et al*., 2002). These models are based on the Euler-Euler formulation, for which the conservation equations of mass, momentum and energy are solved independently for both phases. The coupling between the gas/liquid phases follows directly from the conservation equations and equilibrium conditions at the droplet surface. However, these models assumed that the droplet maintained spherical symmetry during the combustion process, ignoring the effects of the droplet deformation. Based on assumption of axisymmetry, constant liquid density and no gas-phase chemical reaction, Haywood *et al.* (1994a; 1994b) successfully captured the droplet deformation history. Also without the restrictive assumption of spherical shape maintenance, Tanguy *et al*. (2007) modelled the characteristics of droplet combustion for the liquid and gas phases using the "Level Set" and "Ghost Fluid" methods with the constant physical properties assumption.

The aim of this study is to develop a mass transfer model due to vaporization, applicable to the computational fluid dynamics (CFD) calculation in consideration with the droplet surface fluctuation for modeling the droplet combustion process in a temperature-elevated air convective environment. The mass transfer model is implemented into the volume of fluid (VOF) formulation, which is designed for two immiscible fluids where the position of the interface between the fluids is of interest. The mass, momentum and energy conversation equations for both phases, together with the species transfer equation for the gas mixture are solved by assuming axisymmetry, and thus considering droplet shape deformation during the combustion process. The rate of phase change is considered as the source of the gas volume fraction equation, and the generated or departed species from vaporization and chemical reaction are considered as the source of corresponding species transfer equations. The chemical reaction in gas phase is modeled with a one-step finite-rate reaction mechanism, and the gas mixture physical properties are calculated by the kinetic theory as the function of temperature and concentration. The temperature-dependent physical properties for the liquid are also modeled, except the surface tension. The VOF formulation has been used to model the boiling process of a droplet in a convective environment (Hardt and Wondra, 2008) and heated solid surface (Strotos *et al*., 2008). The VOF formulation is in good agreement with the experimental measurement obtained. Comparatively, the present paper is focused on the droplet vaporizing process, while the possible surface boiling is also covered with the same boiling model. The commercial solver Fluent 6.3 is used to solve the sets of equations, and the calculations of the heat and mass transfer between the phases are implemented in the solver via user-defined functions (UDFs). The following assumptions are made in the forthcoming simulations:

1. The droplet maintains constant axisymmetry.

2. The flow field is laminar and also axisymmetrical.

3. The pressure is approximately uniform in the flow field, and the gas mixture density is calculated by the incompressible ideal gas law.

4. Thermal radiation, viscous dissipation and pressure and thermal diffusion are negligible.

5. Thermodynamic equilibrium prevails at the gas-liquid interface.

6. Air is insoluble in the liquid phase.

7. The Marangoni effect, that is, interfacial shear stress caused by the variations of surface tension due to temperature is not modeled. The Marangoni stress has complex effects on the surface liquid motion (Haywood *et al.*, 1994a); however, the numerical calculations for an n-octane droplet by Wu and

Sirignano (2010) showed that the surface temperature and mass transfer rate due to vaporization are modest in the early stages, but diminishes over time in the later period between situations with and without the consideration of surface tension, which is a function of temperature. In this paper, the surface tension in our calculations is a constant, and is considered as a reasonable assumption.

The feasibility and robustness of the CFD VOF formulation for the modeling of the droplet combustion process in a convective environment were evaluated by modeling a decane droplet of an initial diameter of 0.1 mm, which is encountered in a typical spray. The simulation results revealed that during the droplet lifetime, its shape was initially oblate, with its major axis vertical to the mean flow direction. Then it becomes prolate, with its major axis parallel to the mean flow direction, and finally to be oblate again in similar fashion to the first stage when it approaches its vanishing point. The distributions of temperature and molar fraction of species were also presented and analyzed. The results exhibited the capacity and feasibility of CFD methods as a useful tool to model the complex multi physical characteristics of single droplet combustion in convective environment.

2 Physical statement

Fig. 1 shows the schematic of the physical problem, which deals with the combustion of an *n*-decane droplet in a convective air environment. The incoming air comprises 23% oxygen and 77% nitrogen in mass, and enters the computation domain with a uniform free stream velocity (V_{air}) of 0.3 m/s, a free stream temperature (T) of 1000 K and a pressure of 1×10^5 Pa. The whole computation domain is 20 mm long and 5 mm wide, which is believed to be large enough to include the region of influence from the wake and to ensure that the boundary conditions at the far-stream are truly realized (Chiang *et al*., 1992). The droplet is injected into the domain with initial diameter (d_i) of 0.1 mm, temperature (T_i) of 300 K and velocity (V_0) of 0.05 m/s in an opposite direction to the air flow, which gives the droplet an initial Reynolds number of about 0.26, calculated by air physical properties at 1000 K and 1×10^5 Pa. The reaction of the fuel vapor with the oxidizer is assumed to be single-step and irreversible.

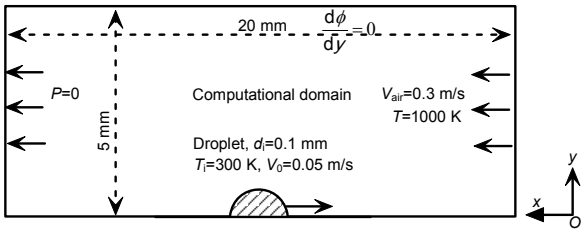

Fig. 1 Schematic of droplet vaporization in a convective air flow

3 Numerical method

3.1 Governing equations

The VOF mathematical formulation for two-phase flow is a single-fluid model and only comprises a set of governing equations for both phases. The fields for all variables and properties are shared by the phases and represent volume-averaged values. The detailed expressions of the conservation equations of mass, momentum, energy, gas phase volume fraction and species as well as the solving strategy are not presented here for brevity, since it has been reported in detail in the Fluent User's Guide (Fluent, 2006). To enclose the sets of the equations for the aforementioned special issues, the chemical reaction rate and the vaporization rate are presented. This is due to the fact that they play a fundamental role in the robustness and accuracy of the combustion process model.

3.2 Chemical reaction model

For the auto-ignited combustion of hydrocarbon in air, the assumed irreversible one-step reaction written in general form is

$$aB + bO_2 \rightarrow cH_2O + dCO_2, \tag{1}$$

where the letter B denotes the reactant, here we choose n-decane ($C_{10}H_{22}$) as the fuel. a, b, c and d are the stoichiometric coefficients. The Arrhenius expressions based on the laminar flow finite-rate model is used to calculate the net source of chemical species R_i, for species B:

$$R_{\mathrm{B}} = -M_{\mathrm{B}} a k_{\mathrm{f}} c_{\mathrm{B}}^{\eta_{\mathrm{B}}} c_{\mathrm{O}_2}^{\eta_{\mathrm{O}_2}}, \tag{2}$$

where M_{B} stands for molecular weight, c_{B} and c_{O_2} are the molar concentrations of decane gas and oxygen, respectively, and η is a rate exponent, η_{B}=0.25 and η_{O_2}=1.5 are used (Westbrook and Dryer, 1981). k_{f} is the forward rate constant and calculated as

$$k_{\mathrm{f}} = n\mathrm{e}^{-E_{\mathrm{r}}/(RT)}, \tag{3}$$

where E_{r} is the chemical activation energy, and n is the reaction pre-exponential factor, n=2.585×10^9 for decane.

3.2 Mass transfer between phases

A vaporization rate model from liquid to gas phase is required to close the conservation equations of energy, species and volume fraction of gas phases. From assumption 6, the total mass transfer per volume from the liquid to gas equals to

$$\dot{m}_{i,\mathrm{v}} = \frac{-M_i D_{i,\mathrm{m}}}{1-x_i} \frac{A_{\mathrm{s}}}{V_{\mathrm{c}}} \frac{\mathrm{d}c_i}{\mathrm{d}l}, \tag{4}$$

where x_i and $D_{i,\mathrm{m}}$ are the molar fraction and diffusion of species i in the gas mixture, respectively, A_{s} is the mass transfer area between phases in cell, m_i is the molecular weight, l is the characteristic length, and V_{c} is the cell volume. The term $\frac{\mathrm{d}c_i}{\mathrm{d}l}$ is approximated as

$$-\frac{\mathrm{d}c_i}{\mathrm{d}l} \approx (c_{i,\mathrm{s}} - c_{i,\mathrm{g}}) / L, \tag{5}$$

where $c_{i,\mathrm{s}}$ and $c_{i,\mathrm{g}}$ are the molar concentrations of species i at liquid surface and gas mixture at the same cell, respectively, and L is the unit cell length. $c_{i,\mathrm{s}}$ is calculated as

$$c_{i,\mathrm{s}} = P_{\mathrm{s}} / (RT), \tag{6}$$

where P_{s} is the saturating pressure corresponding to the local liquid temperature, and T is the local temperature. The total molar concentration of the gas mixture in the cell is

$$c_{\mathrm{t}} = P_{\mathrm{op}} / (RT), \tag{7}$$

where P_{op} is the operating pressure, which is regarded as a known parameter. The molar fraction of species i in the gas mixture is

$$x_i = \frac{Y_i / M_i}{\sum (Y_i / M_i)}, \tag{8}$$

where Y_i is the mass fraction of species i in gas mixture. Combining Eqs. (7) and (8), one obtains the molar concentration of species i at gas phase,

$$c_{i,\mathrm{g}} = x_i c_{\mathrm{t}}. \tag{9}$$

For the computation of the interface area A_{s} in Eq. (4), we relate the interface area to the cell face area A_{c}, expressed for the axisymmetrical system (Fig. 2a), as

$$A_{\mathrm{s}} \approx \alpha_{\mathrm{l}} \alpha_{\mathrm{g}} A_{\mathrm{c}} \approx \alpha_{\mathrm{l}} \alpha_{\mathrm{g}} 2\pi y L, \tag{10}$$

where α_{g} and α_{l} are the volumetric fractions of liquid and gas phases, respectively. When α_{g}=0 or α_{g}=1 in a cell, the interface area between phases equals to zero. Furthermore, when α_{g}=α_{l}=0.5, it approaches a maximum. Substituting Eqs. (5) and (10) into Eq. (4), we can obtain:

$$\dot{m}_{i,\mathrm{v}} = 2\pi y \alpha_{\mathrm{l}} \alpha_{\mathrm{g}} M_i D_{i,\mathrm{m}} (c_{i,\mathrm{s}} - c_{i,\mathrm{g}}) / [(1-x_i) V_{\mathrm{c}}]. \tag{11}$$

An inevitable problem in interfacial flow calculation is that the interface will be smeared over at least one grid cell, induced by fluctuations of the vapor-liquid interface. The smear-out distribution can increase the numerical stabilities; however, it significantly enhances the heat and mass transfer between the phases, resulting in a faster shrinking of the droplet than the process in reality (Hardt and Wondra, 2008). Therefore, to decrease the effects of interface smear-out on the mass and heat transfer, Eq. (11) is further modified by α_{g}. For ideal conditions, as shown

in Fig. 2b, there exists a distinct interface between the phases; the vaporized rate in a specified cell spanning over the interface is strictly calculated by Eq. (4). However, for the conditions of smear-out distribution, as shown in Fig. 2c, a mushy transition zone comprising several cells (for brevity, only two cells are depicted) replaces the distinct interface. The control volume (CV) is adopted to cover the whole transition zone, so the molar flow rate at T–T boundary is still $\dot{n}$; however, that at the s–s boundary consists of (besides the species diffusion) the convective contributions from all interior cells in the CV. It is assumed that the convective contribution from every cell is simply proportional to the gas volume fraction in the cell, which quickly decreases from the cell near liquid phase to that near the gas phase in the transition zone.

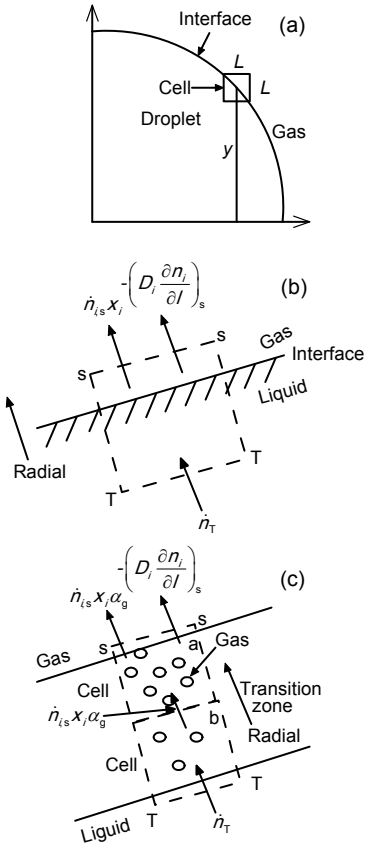

Fig. 2 Schematic for derivation of mass transfer rate due to phase change

(a) One cell spanning over the gas-liquid interface in an axisymmetrical system; (b) Ideal conditions for vaporization in the cell spanning over the interface; (c) Smear-out distribution for interface zone during droplet vaporization

Eq. (11) is thus rewritten as

$$\dot{m}_{i,\mathrm{v}} = Ky\alpha_{\mathrm{l}}\alpha_{\mathrm{g}}\alpha_{\mathrm{g}}M_i D_{i,\mathrm{m}}(c_{i,\mathrm{s}} - c_{i,\mathrm{g}}) / [(1-\alpha_{\mathrm{g}}x_i)V_{\mathrm{c}}]. \quad (12)$$

A constant K=0.1 is introduced to account for the errors during the derivation of Eq. (12), which is found to generate the most accurate transient variance of droplet diameter compared with the experimental data.

A surface boiling model applicable to continuum-field source calculations has been used and verified by Hardt and Wondra (2008) and Kunkelmann and Stephan (2009) for a droplet boiling simulations with the VOF formulation. We also use it to cover the possible situation that the temperature in the most distant cells of the transition zone, where liquid occupies less than 1% of the volume, reaches boiling point. Their model calculates the evaporation mass flux at interface as

$$\begin{aligned} j_{\mathrm{boil}} &= \frac{T_{\mathrm{l}} - T_{\mathrm{s}}}{R_{\mathrm{int}} h_{\mathrm{lv}}}, \\ R_{\mathrm{int}} &= \frac{2-X}{2X}\frac{\sqrt{2\pi R_{\mathrm{gas}}}}{h_{\mathrm{lv}}^2}\frac{T_{\mathrm{s}}^{3/2}}{\rho_{\mathrm{v}}}, \end{aligned} \quad (13)$$

where j_{boil} is the flux since boiling, h_{lv} is the latent heat, T_{l} and T_{s} is the liquid and saturated temperature, respectively. Combining Eqs. (10) and (13), one obtains the boiling mass source per volume as

$$\dot{m}_{i,\mathrm{boil}} = \frac{K_{\mathrm{b}}\alpha_{\mathrm{l}}\alpha_{\mathrm{v}}yL}{V_{\mathrm{c}}}(T_{\mathrm{l}} - T_{\mathrm{s}}) \Bigg/ \left(\frac{2-X}{2X}\frac{\sqrt{2\pi R_{\mathrm{gas}}}}{h_{\mathrm{lv}}}\frac{T_{\mathrm{s}}^{3/2}}{\rho_{\mathrm{v}}} \right), \quad (14)$$

where X is the evaporation coefficient, which has a large degree of uncertainty even for the most common liquid, for example, the range of $10^{-3}<X\leq 1$ for water was suggested by Hardt and Wondra (2008). In this study, X=0.1 is adopted (which corresponds to the value used for water) due to the scarcity of the value for decane. In this light, a constant K_{b} is set to modify the error of using X=0.1, and K_{b}=2, 5, and 10 are pre-calculated, and then the obtained relative variances of burning rate and maximum temperature is less than 3.2%.

3.3 Thermodynamic properties

In the VOF formulation, the variables such as the density, the viscosity and thermal conductivity of the phase mixture are calculated by the fractional presence of the component phases in each control volume (Fluent, 2006).

For gas phase, the mixture density, according to the assumption 3, is computed by the incompressible ideal gas law. The mixture viscosity μ_g and conductivity k_g are both computed using the ideal gas mixture law. And the mixture specific heat capacity is calculated as a mass fraction average of pure species heat capacities. Detailed expressions can be found in (Fluent, 2006).

The viscosity, conductivity and specific heat of individual species are temperature-dependent (NIST website, 2010) (http://webbook.nist.gov/chemistry/fluid/).

Special attention was paid to the decane vapor specific heat calculations, which are conducted in three parts (Fig. 3). Part I is the subcooled vapor zone where the liquid vaporizes below the boiling point, and thus the saturated values corresponding to the liquid temperature are used. Parts II and III are superheated zones, where for temperatures below 600 K the specific heat values are taken from (NIST website, 2010), and for temperatures larger than 600 K the values are calculated by the method mentioned in (Reid, 1987). Note that this method is suggested to be used below 1500 K, but here it is used up to 3000 K because of the absence of data in that temperature range. All of the data are fitted by a polynomial function with the maximum error less than 1.5% (Fig. 3).

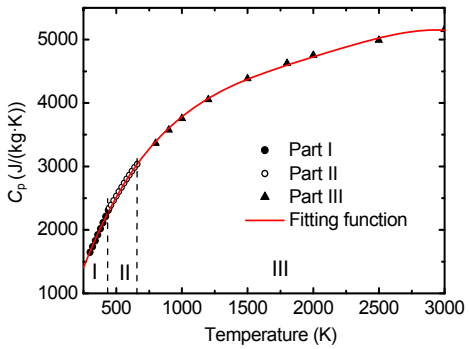

Fig. 3 Specific heat of decane gas vs. temperature
Part I: 300–446.7 K, data from NIST website (2010); Part II: 446.7–600 K, data from NIST website (2010); Part III: >600 K, the method mentioned in (Reid, 1987)

The diffusion coefficient for species i in the gas mixture $D_{i,\mathrm{m}}$ is computed as

$$D_{i,\mathrm{m}} = (1-x_i) \Big/ \sum_{j,j\neq 1} (x_j / D_{ij}), \tag{15}$$

and the modification of the Chapman-Enskog formula (Reid, 1987), which is developed at low to moderate pressure, is used to compute the binary diffusion coefficient D_{ij}.

The physical properties of the liquid decane are functions of temperature only, except surface tension and thermal conductivity. Thermal conductivity is set constant because of its small variation from about 0.13 W/(K·m) at 300 K to 0.11 W/(K·m) at 400 K. According to assumption 7, σ=0.015 N/m is adopted, corresponding to the liquid temperature of 400 K (NIST website, 2010).

4 Modeling process

The simulations adopted a structured four-square grid scheme to ease the calculation of cell face area in Eq. (10). Because the droplet will travel a certain distance before it vanishes, the grids are especially refined in the domain of 1 mm long and 0.08 mm high along its path, inside which the unit cell length is made to be 1.25 μm, so there are 80 grid cells in radial direction inside the droplet. Outside this special domain, the maximum grid cell length is 7.5 μm and the total mesh number for the whole computational domain is 56517. This grid scheme ensures that the length of the cells near the surface always corresponds to 0.0125 times that of the droplet initial diameter of 0.1 mm. This is smaller than the value of 0.02 suggested by Chiang *et al*. (1992) to accurately capture the features of the interface heat and mass transfer in a convective environment. Calculations are first performed on the grid scheme of 60 radial cells inside the droplet, corresponding to the aforementioned value of 0.0167, the $d_{\mathrm{eff}}^2 - t$ error is found to be less than 2% over about 90% of the combustion period. However, as the droplet approaches its vanishing point, the error is significantly increased, mainly due to the fluctuating liquid surface.

The convergence criterion is 10^{-3} for the residual for the continuity equation and the species equations, and 10^{-6} for the energy equation. The time step size is set to be 5 μm, which is smaller than the droplet advective characteristic time in a grid length $t_c=L/v_l$ ≈1.25 (μm)/0.05 (m/s)=25 μs (v_l is the liquid velocity). The pressure-implicit with splitting of operator (PISO) method is used for pressure-velocity coupling, and the pressure computation is by the PRESTO! discretization scheme. The momentum and energy equations were discretized by the second-order and first-order upwind schemes, respectively. The volume fraction equations of species use the geometric reconstruction approach, assuming that the interface between two fluids has a linear slope within each cell, and use this linear shape for calculation of the advection of fluid through the cell faces. To accelerate the convergence, the following under-relaxation factors are: 0.3 for pressure, 0.7 for momentum. The computation is initialized firstly by calculating the two phase flow without a droplet for more than 10 time steps, and then the droplet with its initial conditions is "patched" into the flow field. The total computing time for the case is about 20 h using a 2.2 GB CPU and 2 GB RAM desktop.

5 Model verification

The mass transfer model implemented into CFD VOF formulation is validated by checking the variation of diameter square vs. time with different convective air temperature and velocity. Three cases with the same initial velocity difference of 0.35 m/s, with different air temperatures of 300, 633 and 1000 K are modeled initially. The ignition is realized in the simulations by setting a high-temperature region 0.2 mm in front of the droplet. The region has dimensions of 0.5 mm× 0.2 mm (width×height) and temperature of 1500 K at the beginning (t=0). The initial mass fraction of the n-decane is 0.5 so that the reaction as well as the high temperature can be maintained for an extended period. Fig. 4 shows the simulated results of the cases on the evolution of the square of the droplet equivalent diameter, which is defined as

$$d_{\mathrm{eq}}=(6V_{\mathrm{l}}/\pi)^{1/3}, \tag{16}$$

where V_{l} is the total liquid volume in the whole computational domain, $V_{\mathrm{l}}=\sum_{\mathrm{cell}}\alpha_{\mathrm{l}}V_{\mathrm{c}}$, α_{l} is the liquid volume fraction in the cell. It is observed that d_{eq} expands from t=0 to 0.5 ms since the thermal expansion of the liquid predominates over the vaporization during the initial period. The droplet histories (d_{eq}^2 history) of all cases show approximately linear characteristics, and the transient burning rate defined as $k'=\dfrac{\mathrm{d}d_{\mathrm{eq}}^2}{\mathrm{d}t}$ almost remains constant over the droplet lifetime, which is consistent with the results predicted by the classical theory (Amable and Forman, 1993) based on many simplified assumptions for quiescent droplet combustion. The same linear variation of d_{eq}^2 was also predicted by other numerical calculations for decane droplet with the same initial diameter and ambient temperature as our cases. However, a higher ambient pressure of 1×10^6 Pa was used by Abramzon and Sirignano (1989) and Lage and Range (1993). The experiments conducted by Dietrich *et al*. (2005) on a decane droplet at microgravity environment also exhibited an approximately linear d_{eq}^2 history. The slopes of these lines (k values) in Fig. 4 are, respectively, 1.33 and 1.38 mm^2/s for the air temperature of 300 and 633 K. Xu *et al*. (2003; 2004) showed experimentally that the k value was nearly unaffected by the initial diameter of the droplet if it was in a convective environment, but significantly affected by the air velocity and temperature. From their report, k≈1.25 and 1.3 mm^2/s can be interpolated for the same conditions as the simulations apart from the initial droplet diameters. The small difference of k values between them is considered to be the result of different ignition conditions. If no ignition is applied, it is found that the k value is much larger than its counterpart with ignition when the air temperature is 633 K. The k value for an air temperature of 1000 K is found to be 1.17 mm^2/s in Fig. 4, smaller than the cases with lower air temperatures.

Table 1 shows the comparisons of k values between the experiments and simulations with different relative velocities, while maintaining the same inlet air temperature of 300 K. It is worth mentioning that good agreements are reached for both cases.

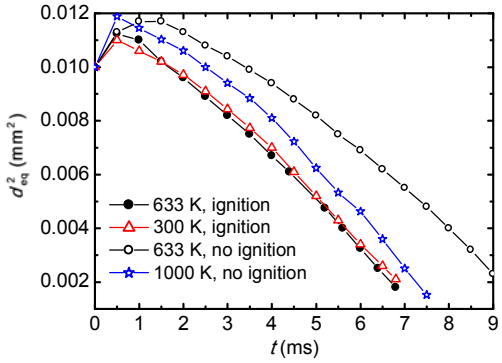

Fig. 4 Square of droplet diameter vs. time with Re_0≈0.26

Table 1 Comparisons of combustion rate constants between experiments and simulations

Method	k (mm^2/s)			
	0.15 m/s*	0.18 m/s	0.26 m/s	0.35 m/s
Experiment	1.00	1.10	1.15	1.25
Simulation	1.04	1.14	1.20	1.33

* Relative velocity. Initial conditions: T_{air}=300 K, d_0=0.1 mm, and $T_{0,d}$=300 K

Additionally, the simulated transient histories of the droplet deformation and the flame structure around the droplet, which will be described in detail in the following paragraphs, are also found to be qualitatively accordant with other numerical observations (Haywood *et al.*, 1994a; Wu and Sirigano, 2010).

6 Results and analysis

Considering the similarity of the results with the three different air temperatures, only the results from T_{air}=1000 K are analyzed in this section. Fig. 5 shows the simulated results of droplet shape at different times, all results are scaled up to the same magnitude for visual comparison. It is found that the transition zone between the liquid and gas phases typically spans about 6–7 cells (for clarity, the grid are not shown in the figures). An interesting phenomenon is the droplet deforming history.

The droplet shape firstly becomes an oblate ellipsoidal shape with major axes vertical to the mean flow direction, then it gradually becomes a prolate shape with major axes parallel to the mean flow direction after about 3 ms. The aspect ratio will reach its

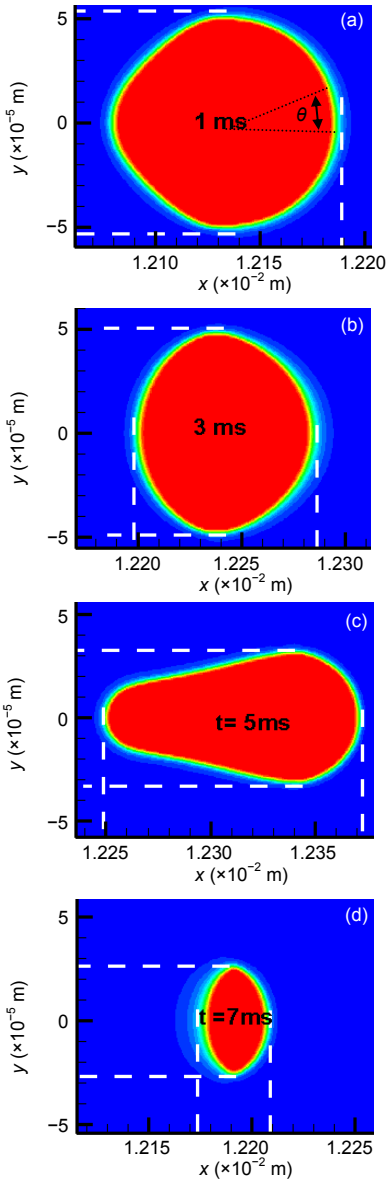

Fig. 5 Simulated results of droplet shape at t=1 ms (a), 3 ms (b), 5 ms (c), and 7 ms (d)
θ is the azimuthal angle

peak value at about 5 ms, and finally it restores to the oblate shape similar to that at the first stage. The reason for this behavior involves many complex physical processes during the droplet lifetime. In general, the stresses exerted on the liquid surface mainly comprise the fluid force due to gas convective flow, and the surface tension and the stress due to evaporation. Haywood *et al.* (1994a) numerically demonstrated that for a deforming droplet, the stress due to evaporation is typically three orders of mag-

nitude smaller than the pressure in the local flow field, implying that the droplet shape is dominated by the surface tension and fluid force. The fluid force includes the pressure within and outside of the liquid, and the pressure due to the droplet deceleration. Here, the shear stress due to gas flow does not directly act on the droplet due to Stefan flow effects for small Reynolds numbers (this will be further illuminated in detail in the following sections), and the Marangoni effects are ignored according to assumption (7). The relative importance of the surface tension effect is measured by the Weber number $We=\rho_l|u_l-u_g|d/\sigma$, where σ is the surface tension, and deformation will occur when We/Re rises towards unity for $Re<<1$ (Brennen, 2005). In the analysis of our cases, $Re\approx0.26$ and $We\approx0.3$ at initial conditions, and thus $We/Re\approx1$, indicating the occurrence of the droplet deformation.

Attention was paid to the static pressure distributions near the droplet, which is shown in Fig. 6. It is found that the pressure at back of the droplet is always larger than that in front of the droplet before 3 ms. According to the well-known Bernoulli equation $P_s+\rho u^2/2=$Const (here gravity term is omitted), the conservation of the dynamic pressure and the static pressure on a streamline for ideal gas has to be abided. Before 3 ms, the heat exchange upwind with the ambient gas mixture is much stronger than the backwind due to a larger relative velocity, so the head-on air is cooled down faster than that at the rear of the droplet. As a result, the cooled air has greater density, pulling the incoming air to accelerate with the penalty of decreased static pressure to keep the pressure balance, and then forms the low pressure zone. Simultaneously, the vaporized gas from the surface is rapidly heated and accelerated due to expansion. However, the gas is damped and decelerated by the head-on air, resulting in impacting pressure due to deceleration, which raises the pressure between the stagnant point and the surface before 3 ms. During the same time, the gas absolute velocity at the rear of the droplet is small because it leaves the surface with a reversed velocity relative to the droplet movement, and thus forms the high pressure. From 3 to 5 ms, the transient temperature distributions shown in Fig. 7 reveal that the flame evolves to an envelope, with the highest temperature quickly rising from 1100 K to 1820 K. The resulting effects are different on the upwind surface and the backwind one. For the upwind and backwind surfaces, the head-on gas exists with a much larger velocity, since the combustion generates more molar products than the reactants. Then, the stagnation point gradually approaches the droplet surface, making the surface pressure increase further. While for the backwind surface, the vaporized gas is accelerated to a downstream position when being heated and expanded; and no impacting pressure is produced since there is no "head-on" air to damp it. Additionally, the absolute velocity of the backward gas leaving the surface is increased due to the deceleration of the

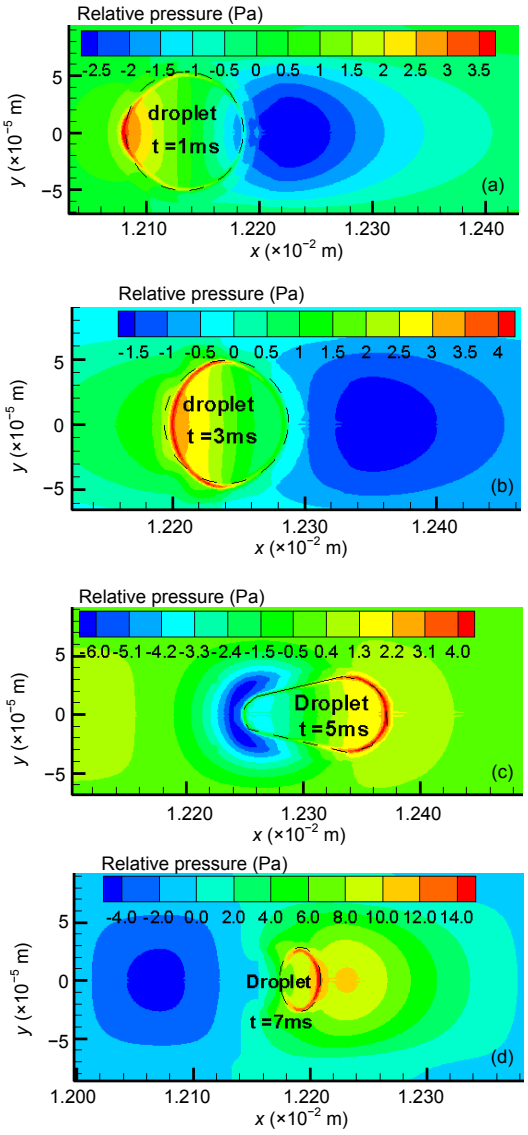

Fig. 6 Transient distribution of static pressure near the droplet at t=1 ms (a), 3 ms (b), 5 ms (c), and 7 ms (d)

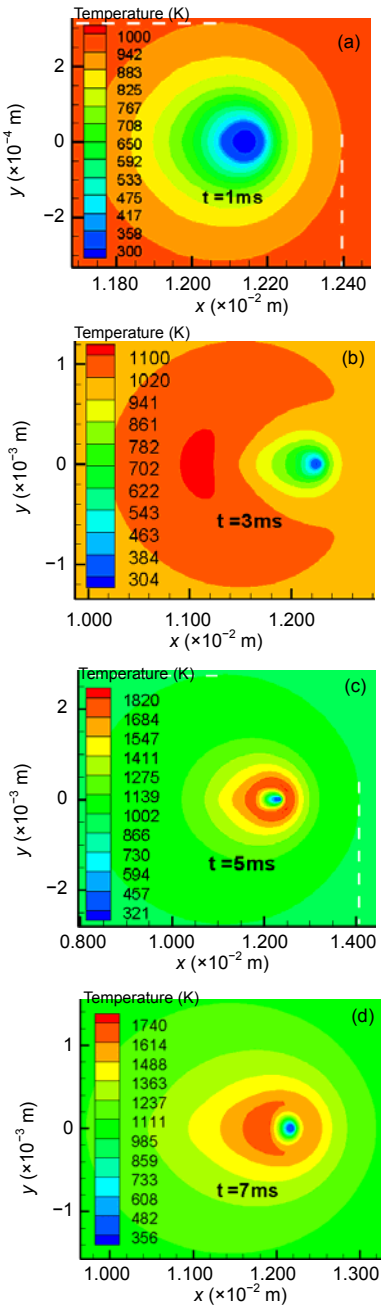

Fig. 7 Temperature fields near the droplet at t=1 ms (a), 3 ms (b), 5 ms (c), and 7 ms (d)

droplet. Thus, it forms a low pressure downstream of the droplet, and the droplet deforms to the prolate with major axes parallel to the mean flow direction primarily due to the anisotropic surface pressure distribution between 3 ms and 5 ms. From 5 ms on, the surface pressure downstream of the droplet is increased. Firstly, this is due to the increased surface tension (Eq. (4)) because of the decreased curvature of the droplet, which always restrains deformation. Secondly, the increased pressure due to droplet acceleration (from 5 ms onwards, the droplet velocity is reversed). Finally, the flame is closer to the droplet as the droplet shrinks, and the combustion products serves as a "head-on" air flow, which arouses a similar impacting pressure and a low pressure zone, as shown in Fig. 6d. The similar histories of the droplet deformation were also observed by Haywood *et al*. (1994a) in their numerical analysis of an *n*-heptane droplet with initial Re=100 and air temperature of 1000 K. Differing from the above explanations, they concluded that the behavior was due to the circulation within the droplet. Their explanation may indeed be appropriate for high Reynolds numbers, but there is no circulation (or too small to see) within the droplet for small Reynolds numbers as we show further below, as a result of the Stefan flow.

The temperature shown in Fig. 7 reflects the difference between the heat generation rate due to chemical reaction and the heat transportation rate from the combustion zone, mainly due to convection. Since the chemical reaction rate is relatively small as there are low values of fuel concentration at the initial stage (<2 ms), the temperature variation in the gas is very small. As the diffusion of fuel vapor increases, the reaction rate subsequently increases, correspondingly, the temperature increases, which further intensifies the gas phase reaction and fuel diffusion from the droplet surface. The outcomes are that the heat release rate as well as the gas phase temperature increases. Furthermore, the gas phase accelerates after ignition. The droplet is first auto-ignited downwind at about 2 ms; here, ignition is simply defined as the first appearance of a significant temperature increases with time. This early combustion stage is a so-called "rear flame", as shown in Fig. 7b. And then, the flame gradually spreads from the rear to envelope the whole droplet, becoming an "envelope flame" (Figs. 7c and 7d). Recently, Wu and Sirignano (2010) numerically found that an initial wake flame will always be transitioned into an envelope flame. They also concluded that the initial Damkohler number (Da_0=(d_0/u_∞)/($\rho_\infty Y_F^0$/($\omega_0 M_f$)))=1.02 (ω_0 is the chemical reaction rate), can be used to judge the initial shape of flame for n-octane fuel at 2×10^6 Pa pressure

and 1500 K ambient temperature. Although the ambient conditions in this study are quite different from those of the aforementioned studies, the results (Da_0<1) obtained seem to be qualitatively accordant with the conclusions. Fig. 7 also shows that the highest temperature in the flame transfers from the droplet rear to the front, and finally returns to the rear again, as mainly determined by the available oxygen. The reaction rate, as well as the temperature, falls gradually as the droplet approaches its vanishing point, as a result of the decreased fuel concentration.

Fig. 8 and Fig. 9 respectively show the temperature and mass transfer rate due to phase change around the gas-liquid interface at different times, as a function of azimuthal angle θ, here, θ=0 is at the upstream stagnation point and the coordinate of the origin is the arithmetic average of the two droplet boundary endpoints on the axis (Fig. 5). The droplet boundary is adopted based on the criteria of 10% liquid volumetric fraction (α_l=0.1). It is observed that the mass transfer rate always keeps in phase with the temperature variations. The curves of local heat and mass transfer look zigzag, especially when the droplet becomes, to most extent, a prolate shape at t=5 ms. It implies that the shear force from the air flow, which always smoothens the distributions of the surface temperature, as well as the mass transfer rate, is small for our cases. When the droplet becomes an oblate shape with major axes vertical to the mean flow direction at t=3 and 7 ms, the transverse top point (θ=90°) has the maximum temperature and mass transfer rate. When the droplet becomes a prolate shape with major axes parallel to the mean flow at t=5 ms, the end points on the symmetrical axis (θ=0°, 180°) have the maximum temperature and mass transfer rate; moreover, they always have almost the same values during the droplet lifetime.

Fig. 10 presents the molar concentration of decane vapor around the droplet at different times, which can be used to approximately determine the flame structure in consideration of the combustion controlled by the species diffusion. Thus, the decane species cannot escape beyond the boundaries of the flame. Comparing temperature contours in Fig. 7, the boundary of about 2% decane vapor molar concentration in Fig. 10 approximately corresponds to the flame inner boundary close to droplet. Table 2 shows

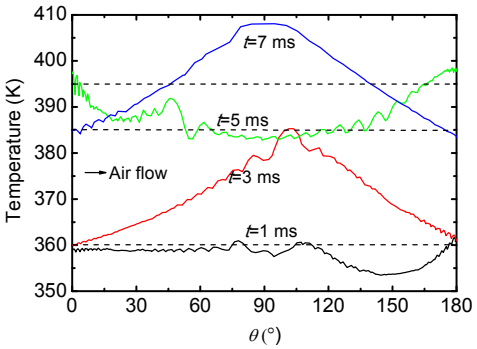

Fig. 8 Temperature distributions along the gas-liquid interface for different times, Re_0≈0.26, and T_{air}=1000 K

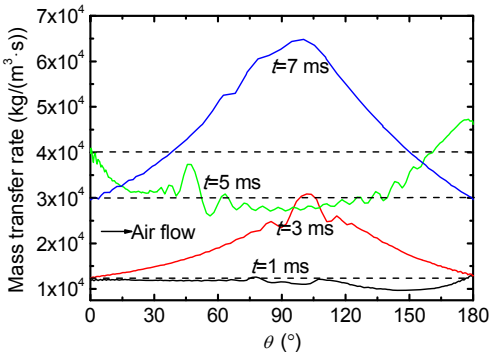

Fig. 9 Mass transfer rate along the gas-liquid interface for different times, Re_0≈0.26, and T_{air}=1000 K

the "flame" geometrics at different times, where the definition of l_x and l_y is depicted in Fig. 10. It is found that l_x/d_{eq} and l_y/d_{eq} always decrease as time increases for our case, implying that the flame shrinks much faster than the droplet when the droplet approaches its vanishing point. While the aspect ratio of the flame (l_x/l_y) is closely relative to the droplet shape, both of which synchronously reach peak value at t=5 ms.

Fig. 11 shows the typical velocity vector near the droplet at t=1 ms. The flow field is affected by the head-on air velocity, the thermal effects on the properties, and the species flows due to the reactions. The so-called Stefan flow outside the droplet surface, which is the movement of the chemical species by the gas that is induced to flow by the production or removal of the species at the droplet interface, is clearly observed. By observing the flow fields at different times, it is found that the air velocity ahead of the frontal stagnation point before 3 ms is larger than that of the far-field one. After 3 ms, the maximum velocity transfers to the downwind of the droplet, accounting for the formation of low pressure upstream and

Table 2 Flame extension of droplet combustion

t (ms)	l_x (mm)	l_y (mm)	d_{eq} (mm)	l_x/d_{eq}	l_y/d_{eq}	l_x/l_y
3	0.65	0.54	0.097	6.70	5.57	1.20
5	0.50	0.40	0.079	6.33	5.06	1.25
7	0.26	0.24	0.050	5.20	4.80	1.08

t: time; l_x: axial length; l_y: transverse length; T_{air}=1000 K, Re_0≈0.26, d_0=0.1 mm, $T_{0,d}$=300 K

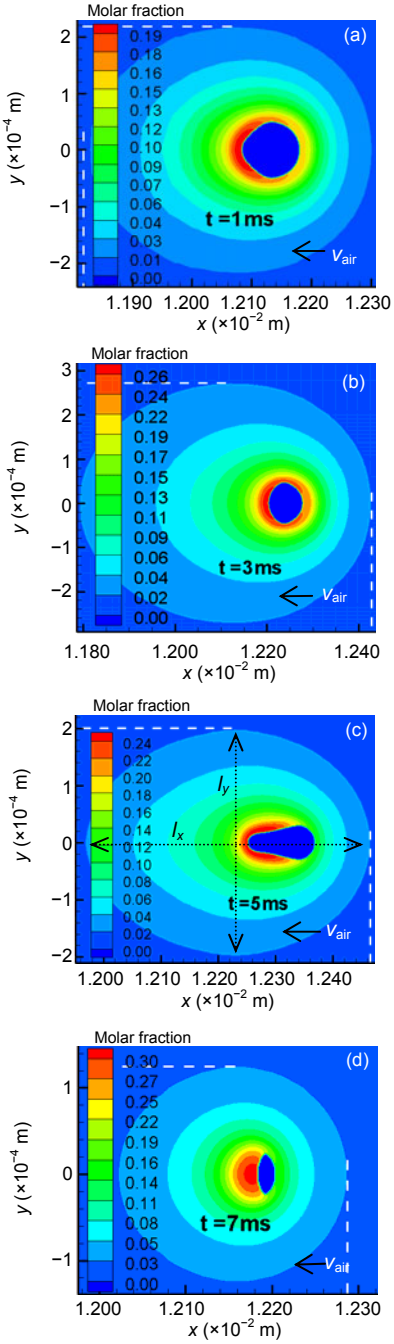

Fig. 10 Molar fraction of decane around the droplet at t=1 ms (a), 3 ms (b), 5 ms (c), and 7 ms (d)
The dark blue region in the center is liquid decane

downstream of the droplet at different times for the conservation of total pressure. The droplet is firstly accelerated before 3 ms, then decelerated from 3 ms to about 5 ms. At about 5 ms, it is completely reversed, and from then on, it is accelerated. The velocity reaches 0.15 m/s at 7 ms.

The flow path lines in both liquid and gas phases near the droplet are depicted in Fig. 12, with the color denoting the liquid volume fraction. The lines start from the air inlet boundary and the droplet central surface vertical to the symmetrical axis. The arrows on the other hand stand for the flow direction. A unique phenomenon is that there is no clear circulation inside the droplet to be observed, which seemingly disagrees with comments in previous studies (Renksizbulut and Haywood, 1988; Haywood *et al.*, 1994a). They ascribed the circulations inside the droplet to tangential stress from the continuum phase. This is indeed true for high Reynolds numbers in which the Stefan flow is not strong enough to resist the gas flow effects, as mainly determined by the

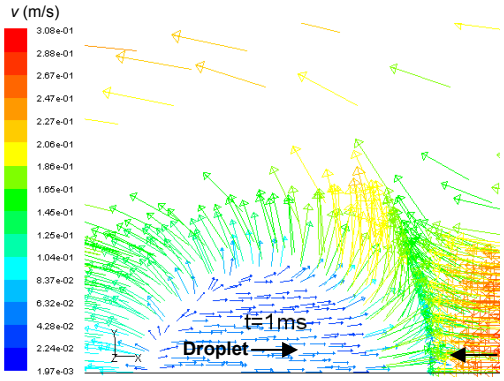

Fig. 11 Typical velocity vector near the droplet at t=1 ms, Re_0≈0.26, and T_{air}=1000 K

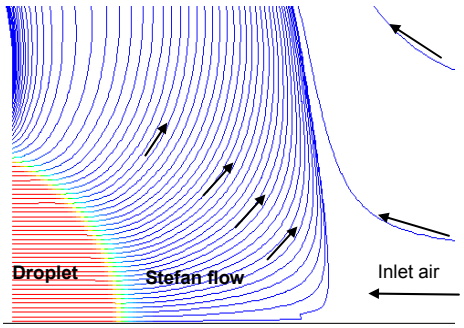

Fig. 12 Path lines colored by liquid volume fraction
Lines start from the air inlet boundary and the droplet central surface vertical to the axis. Re_0≈0.26 and T_{air}=1000 K

liquid/gas density ratio, vaporization rate, and ambient Reynolds number. While for low Reynolds numbers, Figs. 11 and 12 reveal that the Stefan flow prevents the liquid from being in direct contact with the head-on air, and it assimilates the tangential stress due to the change of air flow direction. In the VOF formulation, the velocity direction of vapor just leaving the liquid surface is defined in the same manner as the liquid one in the same cell, referring to the momentum conservation equation. Therefore, the Stefan flow itself has little effect on the tangential movement of liquid at surface. Thus, it's reasonable and possible that the circulation inside the droplet does not exist for the low Reynolds numbers, in which the Stefan flow prevails over the air flow near the droplet surface.

7 Conclusions

The general CFD simulating results of a single pure-component droplet creeping in a temperature-elevated convective air flow (Re_0=0.26) were analyzed based on the VOF formulation. The numerical model did not depend on the assumption of spherical symmetry, and solved the conservation equations for both gas and liquid phases with temperature and component dependent physical properties for gas phase. The chemical reaction was also modeled with the one-step finite-rate mechanism. The simulated results verified the capability and feasibility of CFD analysis for the complex multi-physical coupling process of droplet combustion. The main conclusions from the simulations on droplet combustion process can be drawn:

1. The square of the droplet equivalent diameter changes in a non-linear fashion with time; and the burning constants with different air temperatures were comparable with the experimental results. The volume that increases due to thermal liquid expansion at the initial stages of droplet propagation was also captured.

2. The droplet shape firstly deforms to the oblate shape with major axes vertical to mean flow direction, and to the prolate shape with major axes parallel to mean flow direction, and finally restores to the oblate shape. The same phenomena were also reported by other numerical calculations for high Reynolds numbers. However, they have different aerodynamic mechanism. For the low Reynolds case, it is mainly ascribed to the pressure field and surface tension, while for the high Reynolds case, it is mainly ascribed to the circulation inside the droplet.

3. The rear flame is first observed at about 2 ms after the droplet is injected into the convective air, and at about 5 ms, the flame evolves to an envelope one. Simultaneously, the maximum temperature also shifts from the back to the frontal, finally, it returns to the back before the droplet vanishes. The availability of oxygen is considered to be the culprit of the flame behavior aforementioned.

4. When the droplet extrudes relative to a sphere, there is maximum of surface temperature and mass transfer rate due to phase change. Both values for the end points on the symmetrical axis keep almost the same during the lifetime.

5. The flame shrinks faster than the droplet when it approaches its vanishing point.

6. The Stefan flow near the droplet surface is well captured, which prevails over the air flow near the gas/liquid interface, and assimilates the tangential stress from the air flow, resulting in disappearance of the circulation inside the droplet.

References

Abramzon, B., Sirignano, W.A., 1989. Droplet vaporization model for spray combustion calculations. *International Journal of Heat and Mass Transfer*, **32**(9):1605-1618. [doi:10.1016/0017-9310(89)90043-4]

Abramzon, B., Sazhin, S., 2005. Droplet vaporization model in the presence of thermal radiation. *International Journal of Heat and Mass Transfer*, **48**(9):1868-1873. [doi:10.1016/j.ijheatmasstransfer.2004.11.017]

Amable, L., Forman, A.W., 1993. Fundamental Aspects of Combustion. Oxford University Press, New York, Oxford.

Brennen, C.E., 2005. Fundamentals of Multiphase Flow. Cambridge University Press.

Chiang, C.H., Raju, M.S., Sirignano, W.A., 1992. Numerical analysis of convecting vaporizing fuel droplet with variable properties. *International Journal of Heat and Mass Transfer*, **35**(5):1307-1324. [doi:10.1016/0017-9310(92)90186-V]

Cuoci, A., Mehl, M., Ferraris, G.B., Faravelli, T., Manca, D., Ranzi, E., 2005. Autoignition and burning rates of fuel droplets under microgravity. *Combustion and Flame*, **143**(3):211-226. [doi:10.1016/j.combustflame.2005.06.003]

Dash, S.K., Som, S.K., 1991. Ignition and combustion of liquid fuel droplet in a convective medium. *Journal of Energy Resources Technology*, **113**(3):165-170. [doi:10.1115/1.2905799]

Dgheim, J., Chesneau, X., Pietri, L., Zeghmati, B., 2002. Heat and mass transfer correlations for liquid droplet of a pure fuel in combustion. *Heat and Mass Transfer*, **38**(7-8):543-550. [doi:10.1007/8002310100202]

Dietrich, D.L., Struk, P.M., Ikegami, M., Xu, G., 2005. Single droplet combustion of decane in microgravity: experiments and numerical modeling. *Combustion Theory and Modelling*, **9**(4):569-585. [doi:10.1080/13647830500256039]

Fluent, 2006. Fluent 6.3 Documents. Fluent Incorporation.

Hardt, S., Wondra, F., 2008. Evaporation model of interfacial flows based on a continuum-field representation of the source terms. *Journal of Computational Physics*, **227**(11):5871-5895. [doi:10.1016/j.jcp.2008.02.020]

Haywood, R.J., Renksizbulut, M., Raithby, G.D., 1994a. Numerical solution of deforming evaporating droplets at intermediate Reynolds numbers. *Numerical Heat Transfer, Part A: Applications*, **26**(3):253-272. [doi:10.1080/10407789408955991]

Haywood, R.J., Renksizbulut, M., Raithby, G.D., 1994b. Transient deformation and evaporation of droplets at intermediate Reynolds numbers. *International Journal of Heat and Mass Transfer*, **37**(9):1401-1409. [doi:10.1016/0017-9310(94)90186-4]

Jog, M.A., Ayyaswamy, P.S., Cohen, I.M., 1996. Evaporation and combustion of a slowly moving liquid fuel droplet: higher-order theory. *Journal of Fluid Mechanics*, **307**:135-165. [doi:10.1017/S0022112096000079]

Kunkelmann, C., Stephan, P., 2009. CFD simulation of boiling flows using the volume-of-fluid method within OPENFOAM. *Numerical Heat Transfer, Part A: Applications*, **56**(8):631-646. [doi:10.1080/10407780903423908]

Lage, P.L.C., Range, R.H., 1993. Single droplet vaporization including thermal radiation absorption. *Journal of Thermophysics and Heat Transfer*, **7**(3):502-508. [doi:10.2514/3.446]

Lior, N., Sarmiento-Darkin, W., Al-Sharqawi, H.S., 2006. The exergy fields in transport processes: Their calculation and use. *Energy*, **31**(5):553-578. [doi:10.1016/j.energy.2005.05.009]

Madooglu, K., Karagozian, A.R., 1993. Burning of a spherical fuel droplet in a uniform flowfield with exact property variation. *Combustion and Flame*, **94**(3):321-329. [doi:10.1016/0010-2180(93)90077-G]

Reid, R.C., 1987. The Properties of Gases and Liquids, 4th Edition. McGraw-Hill Inc, p.167-172.

Renksizbulut, M., Yuen, M.C., 1983. Numerical study of droplet evaporation in a high-temperature stream. *Journal of Heat Transfer*, **105**(2):389-397. [doi:10.1115/1.3245591]

Renksizbulut, M., Haywood, R.J., 1988. Transient droplet evaporation with variable properties and internal circulation at intermediate Reynolds numbers. *International Journal of Multiphase Flow*, **14**(2):189-202. [doi:10.1016/0301-9322(88)90005-5]

Shaygan, N., Prakash, S., 1995. Droplet ignition and combustion including liquid-phase heating. *Combustion and Flame*, **102**(1-2):1-10. [doi:10.1016/0010-2180(95)00027-4]

Strotos, G., Gavaises, M., Theodorakakos, A., Berleges, G., 2008. Numerical investigation on the evaporation of droplets depositing on heated surfaces at low Weber numbers. *International Journal of Heat and Mass Transfer*, **51**(7-8):1516-1529. [doi:10.1016/j.ijheatmasstransfer.2007.07.045]

Talley, D.G., Yao, S.C., 1988. A Semi-Empirical Approach to Thermal and Composition Transients inside Vaporizing Fuel Droplets. Symposium (International) on Combustion, **21**(1):609-616. [doi:10.1016/S0082-0784(88)80291-1]

Tanguy, S., Menard, T., Berlemont, A., 2007. A level set method for vaporizing two-phase flows. *Journal of Computational Physics*, **221**(2):837-853. [doi:10.1016/j.jcp.2006.07.003]

Westbrook, C.K., Dryer, F.L., 1981. Simplified reaction mechanisms for the oxidation of hydrocarbon fuels in flames. *Combustion Science and Technology*, **27**(1-2):31-43. [doi:10.1080/00102208108946970]

Wu, G., Sirigano, W.A., 2010. Transient burning of a convective fuel droplet. *Combustion and Flame*, **157**(5):970-981. [doi:10.1016/j.combustflame.2009.11.019]

Xu, G.W., Ikegami, M., Honma, S., Ikeda, K., Ma, X.X., 2003. Inverse influence of initial diameter on droplet burning rate in cold and hot ambiences: a thermal action of flame in balance with heat loss. *International Journal of Heat and Mass Transfer*, **46**(7):1155-1169. [doi:10.1016/S0017-9310(02)00397-6]

Xu, G.W., Ikegami, M., Honma, S., Ikeda, K., Dietrich, D.L., 2004. Interactive influence of convective flow and initial droplet diameter on isolated droplet burning rate. *International Journal of Heat and Mass Transfer*, **47**(8-9):2029-2035. [doi:10.1016/j.ijheatmasstransfer.2003.09.035]